Inorganic Chemistry
Communication
Cite This: Inorg. Chem. 2019, 58, 14998−15003
pubs.acs.org/IC

Redox Tuning via Ligand-Induced Geometric Distortions at a YMn_3O_4 Cubane Model of the Biological Oxygen Evolving Complex

Heui Beom Lee[†] and Theodor Agapie*[,†]

[†]Department of Chemistry and Chemical Engineering, California Institute of Technology, 1200 E. California Blvd MC 127-72, Pasadena, California 91125, United States

Supporting Information

ABSTRACT: The function of proteins involved in electron transfer is dependent on cofactors attaining the necessary reduction potentials. We establish a mode of cluster redox tuning through steric pressure on a synthetic model related to Photosystem II. Resembling the cuboidal $[CaMn_3O_4]$ subsite of the biological oxygen evolving complex (OEC), $[Mn_4O_4]$ and $[YMn_3O_4]$ complexes featuring ligands of different basicity and chelating properties were characterized by cyclic voltammetry. In the absence of ligand-induced distortions, increasing the basicity of the ligands results in a decrease of cluster reduction potential. Contraction of Y-oxo/Y−Mn distances by 0.1/0.15 Å enforced by a chelating ligand results in an increase of cluster reduction potential even in the presence of strongly basic donors. Related protein-induced changes in Ca-oxo/Ca−Mn distances may have similar effects in tuning the redox potential of the OEC through entatic states and may explain the cation size dependence on the progression of the S-state cycle.

Through processes such as photosynthesis and respiration, electron transfer (ET) is fundamental to life.[1] In addition to controlling the rate of ET, tuning the redox potential of ET mediators can regulate biological reactions.[2−5] Factors that tune the redox potentials of metallocofactors include: (1) oxidation state and geometry of the metal center(s),[6,7] (2) ligands in the primary coordination sphere,[8,9] (3) secondary coordination sphere interactions such as hydrogen bonding and polarity of the medium,[10−14] and (4) binding of regulatory molecules.[15] Featuring a $[CaMn_4O_5]$ core, the oxygen evolving complex (OEC) of Photosystem II catalyzes the 4 e^-/4 H^+ oxidation of H_2O to O_2.[16−18] The mechanism of O−O bond formation and the role of the redox-inactive Ca^{2+} ion have been the subject of numerous biochemical, spectroscopic, computational, and synthetic studies, but the role of Ca^{2+} remains unclear.[19−33] Removal of Ca^{2+} has a minimal effect on the $[Mn_4O_5]$ core structure.[23] Substitution of Ca^{2+} with other metal ions has distinct outcomes. Incorporation of alkali metals reveals a cation size dependence in the $S_1 \rightarrow S_2$ one e^- oxidation step: Li^+ and Na^+ supplemented samples show the multiline EPR signal characteristic of the S_2 state, while K^+, Rb^+, and Cs^+ supplemented samples do not show formation of the S_2 state, suggesting that the redox properties of the OEC are affected by the size of the redox-inactive metal.[34] Notably, turnover is inhibited by substitution of Ca^{2+} with other metal ions with the exception of Sr^{2+},[35] providing opportunities for mechanistic insight through systematic structure−function studies on model complexes.

Studies on synthetic heterometallic complexes featuring acetate-bridged $[MMn_3O_4]$, $[MMn_3O(OH)]$, and $[MFe_3O(OH)]$ cores with redox-inactive metal ions M = Ca^{2+}, Sr^{2+}, Zn^{2+}, Y^{3+}, Ln^{3+}, and Sc^{3+} have shown that cluster reduction potentials correlate linearly with the pK_a of the metal aqua ion: the least acidic Ca^{2+}- and Sr^{2+}-containing clusters in the series have the lowest reduction potentials.[31,36−41] For the series of $[Ln^{3+}Mn_3O_4]$ complexes, redox potential is also found to correlate linearly with the ionic radii of the lanthanides with the larger, less acidic lanthanide-containing clusters having lower reduction potentials.[38] Theoretical studies on the cuboidal $[MMn_3O_4]$ model complexes have validated the correlation between redox potential and the Lewis acidity of the redox-inactive metal ion; however, calculations also suggest that such correlation does not hold for the OEC, which is proposed to respond only to the charge of the redox-inactive metal ion.[42] Dinuclear examples have been reported in which redox inactive metal ions not only influence the redox potential of the transition metal, but also modulate the reactivity of oxo, peroxo, and other metal bound moieties.[43−50] In several cluster and bimetallic systems, correlations are observed between reduction potentials or rates of reaction and Lewis acidity of redox inactive metals.[31,36,38,39,51−55] Other systems show dependence between redox chemistry and the charge of the cation, not its Lewis acidity;[42,46] notably, such systems have constrained binding environments such as the protein cavity for the OEC or pendant crown ethers. Finally, correlations involving the Lewis acidity or the charge of the redox-inactive metal both fail to address the cation size dependence experimentally observed in the OEC: larger, less acidic alkali metals inhibit the $S_1 \rightarrow S_2$ oxidation.[34]

Herein, we report the synthesis, crystal structure, electrochemical characterization, and comparison of $[Mn_4O_4]$ and $[YMn_3O_4]$ complexes featuring bridging ligands of different basicity and chelating properties. We demonstrate that geometric pressure imposed by a chelating ligand results in contraction of metal-oxo distances, leading to an increase in cluster reduction potential despite the presence of more electron-rich ligands. We propose that related changes in Ca-oxo/Ca−Mn distances driven by the protein active site cavity may have a similar effect in tuning the redox potential of the

Received: February 20, 2019
Published: May 16, 2019

DOI: 10.1021/acs.inorgchem.9b00510
Inorg. Chem. 2019, 58, 14998−15003

Scheme 1. Synthesis of $[Mn_4O_4]$ and $[YMn_3O_4]$ Complexes Studied in This Work

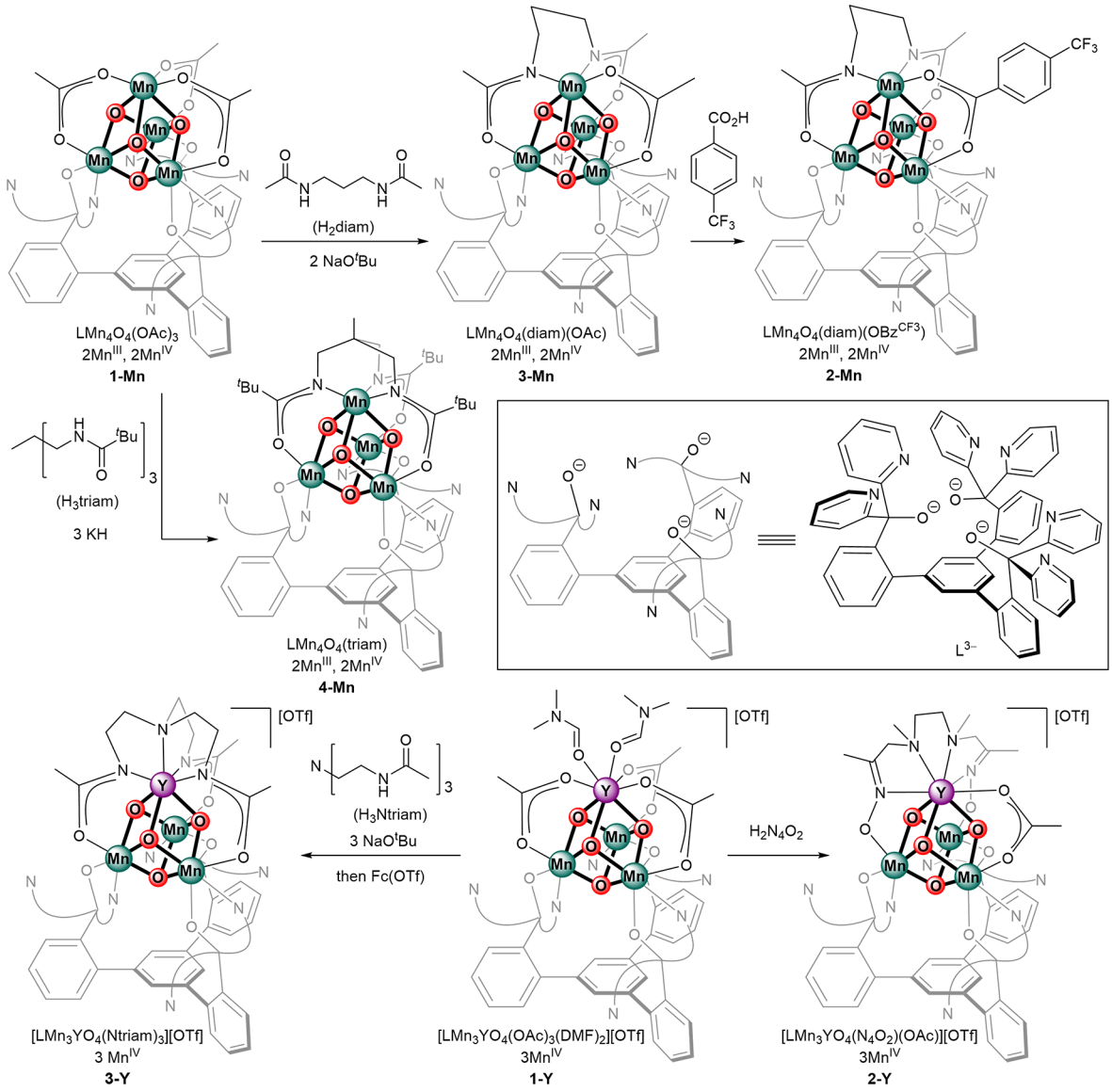

OEC. A similar effect may explain the cation size dependence in the $S_1 \rightarrow S_2$ oxidation, whereby the cavity surrounding the OEC may enforce nonequilibrium metal-oxo distances that impact the reduction potential of the OEC.

To investigate the effect of ligand basicity in modulating cluster reduction potential, $[Mn_4O_4]$ complexes featuring carboxylate and amidate bridging ligands were synthesized (Scheme 1). Treatment of the previously reported $LMn_4O_4(OAc)_3$ complex **1-Mn** with a tethered diamidate ligand results in the formation of $LMn_4O_4(diam)(OAc)$ (**3-Mn**).[56] Subsequent treatment of **3-Mn** with *p*-CF_3-benzoic acid results in the formation of $LMn_4O_4(diam)(OBz^{CF3})$ (**2-Mn**).[56] Complexes **1-Mn** ∼ **3-Mn** are nearly isostructural with respect to the Mn-oxo distances; the $[Mn_2^{III}Mn_2^{IV}]/[Mn^{III}Mn_3^{IV}]$ couple is observed at +250, −15, and −150 mV vs Fc/Fc^+, respectively.[37,56] Toward further decreasing the potential of this redox couple, a triamidate-supported $[Mn_4O_4]$ cluster was targeted (Scheme 1). Deprotonation of H_3triam with KH followed by treatment with **1-Mn** results in the formation of **4-Mn**. The crystal structure of **4-Mn** is consistent with the LMn_4O_4(triam) formulation (Figure 2a). The reversible $[Mn_2^{III}Mn_2^{IV}]/[Mn^{III}Mn_3^{IV}]$ couple is observed at −465 mV vs Fc/Fc^+, representing a shift of 600 mV relative to **1-Mn** (Figure S13). Treatment of **4-Mn** with Ag(OTf) affords the one electron oxidized species $[LMn_4O_4(triam)][OTf]$ (**4-Mn-ox**). In a related series of $[Co_4O_4]$ cuboidal systems, cluster reduction potentials were found to be inversely proportional to the weighted sum of ligand pK_a's (effective basicity) in H_2O.[57] A similar correlation can be obtained for **1-Mn** ∼ **4-Mn** using the pK_a of HOAc (12.6), *p*-CF_3–$C_6H_4CO_2H$ (9.6), and *N*-methylacetamide (25.9) in DMSO with a slope of −70 mV/pK_a (Figure 1, Table S3), establishing a linear trend between ligand basicity and cluster potential in $[Mn_4O_4]$ complexes.[58−61]

To investigate the effect of ligand basicity in modulating the reduction potential of clusters featuring redox-inactive metals, $[YMn_3O_4]$ complexes supported by different bridging ligands were targeted (Scheme 1). For $[LYMn_3O_4(OAc)_3]^+$ (**1-Y**), the $[YMn_3^{IV}]/[YMn^{III}Mn_2^{IV}]$ couple is observed at −430 mV vs Fc/Fc^+.[39] Treatment of **1-Y** with Cp^*_2Fe results in the formation of the one electron reduced complex $[LYMn_3O_4(OAc)_3]$ (**1-Y-red**).[62] Treatment of **1-Y** with

DOI: 10.1021/acs.inorgchem.9b00510
Inorg. Chem. 2019, 58, 14998−15003

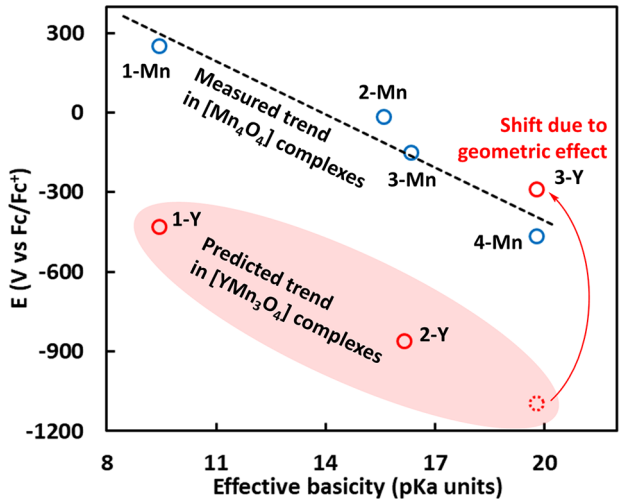

Figure 1. Linear correlation between redox potential and effective ligand basicity in $[Mn_4O_4]$ complexes **1-Mn** ∼ **4-Mn**. Similar trend based on ligand basicity observed for $[YMn_3O_4]$ complexes **1-Y** and **2-Y**. Deviation from the trend in **3-Y** attributed to a geometric effect described in this study.

1 equiv of a chelating bis-oxime proligand ($H_2N_4O_2$) results in the formation of **2-Y**. The crystal structure of **2-Y** is consistent with the $[LYMn_3O_4(N_4O_2)(OAc)(DMF)][OTf]$ formulation (Figure 2b).[63] Despite the pK_a difference of 13 units between acetic acid and acetoxime (pK_a = 25.2)[64] moieties, the reaction is thought to be driven by a kinetic chelate effect. For **2-Y**, the reversible $[YMn_3^{IV}]/[YMn^{III}Mn_2^{IV}]$ couple is observed at −860 mV vs Fc/Fc^+ (Figure S15). The bis-oximate ligand decreases the reduction potential of **2-Y** by 430 mV relative to that of **1-Y**, consistent with the increased basicity of the oximate donors compared to acetates. The difference in redox potential between **1-Y** and **2-Y** is similar to that between **1-Mn** and **3-Mn**, suggesting that a similar trend based on effective ligand basicity may be operative in $[YMn_3O_4]$ complexes.

On the basis of the effective basicity trend, a triamidate-supported $[YMn_3O_4]$ complex was targeted to further decrease the potential of the $[YMn_3^{IV}]/[YMn^{III}Mn_2^{IV}]$ couple. Due to the larger size of Y compared to Mn, triam^{3-} was not suitable as a supporting ligand. However, treatment of **1-Y** with a tren-based triacetamide proligand (H_3Ntriam) and 3 equiv of NaO^{t}Bu results in the formation of the amidate-supported, one electron reduced complex **3-Y-red** (Scheme 1). The ESI-MS peak at m/z = 1443 is consistent with the mass of $[LYMn_3O_4(Ntriam)]^+$ (Figure S10). For **3-Y-red**, the reversible $[YMn_3^{IV}]/[YMn^{III}Mn_2^{IV}]$ couple is observed at −290 mV vs Fc/Fc^+ (Figure S17). Accordingly, treatment of **3-Y-red** with (Fc)(OTf) leads to the formation of the one electron oxidized complex **3-Y**. The crystal structure of **3-Y** is consistent with the $[LYMn_3O_4(Ntriam)][OTf]$ formulation (Figure 2c). Despite the similarity in pK_a for acetoxime and acetamide moieties and the increased effective ligand basicity in **3-Y**, the tris-amidate ligand increases the reduction potential of **3-Y** by 140 mV relative to that of **1-Y**, inconsistent with the increased basicity of the amidate donors compared to acetates.

To obtain a rationale for the shifts in redox potential observed in **1-Y** ∼ **3-Y**, metal-oxo and metal−metal distances were compared among the series of oxidized and reduced complexes (Table 1). Comparing the reported crystal

Table 1. Y-oxo and Y−Mn Distances (Å) in Complexes 1-Y-red, 1-Y, 2-Y, and 3-Y[a]

	1-Y-red	1-Y	2-Y	3-Y
Y(1)−O(1)	2.297(3)	2.432(2)	2.308(2)	2.289(4)
Y(1)−O(2)	2.344(3)	2.335(2)	2.396(2)	2.278(4)
Y(1)−O(3)	2.306(3)	2.389(2)	2.422(3)	2.289(4)
Y−O average	2.316(3)	2.385(2)	2.375(2)	2.285(4)
Y(1)−Mn(1)	3.212(1)	3.239(1)	3.181(1)	3.106(1)
Y(1)−Mn(2)	3.144(1)	3.298(1)	3.193(1)	3.119(1)
Y(1)−Mn(3)	3.192(1)	3.213(1)	3.295(1)	3.100(1)
Y−Mn average	3.183	3.250(1)	3.223(1)	3.108(1)

[a]Average distances underlined for emphasis.

structures of **1-Y-red** and **1-Y**, a slight contraction of Y-oxo and Y−Mn distances is observed in **1-Y-red**.[39,62] This contraction can be rationalized in terms of the increased basicity of the bridging oxos in the reduced cluster, resulting in the observed Y-oxo/Y−Mn contraction. Comparing the structures of **1-Y** and **2-Y**, the average Y-oxo and Y−Mn distances differ only by about 0.01 and 0.03 Å, respectively. Therefore, binding of the bis-oximate ligand does not significantly change the geometry of the $[YMn_3O_4]$ core, and the decrease in reduction potential of **2-Y** relative to that of **1-**

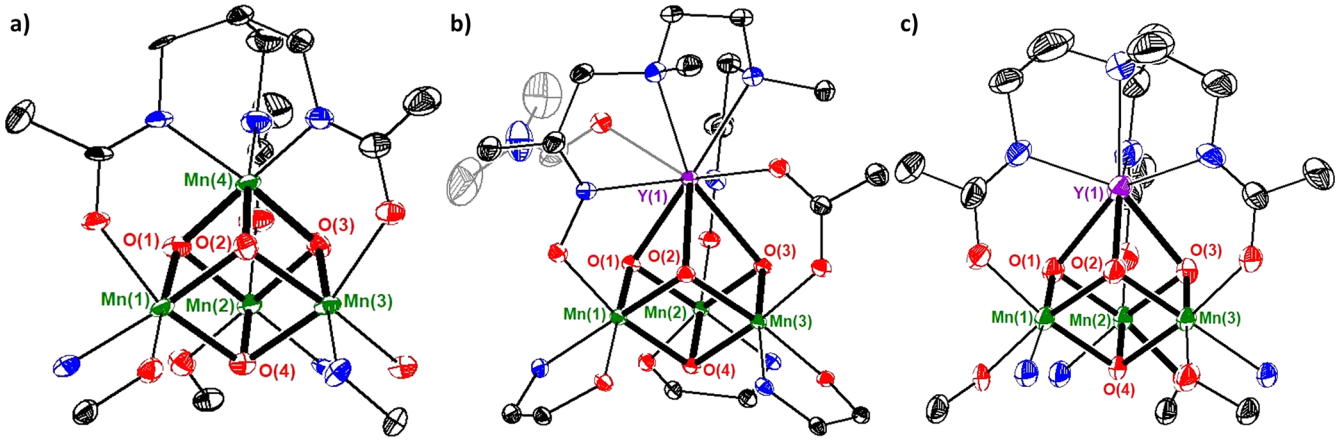

Figure 2. Truncated crystal structures of (a) **4-Mn**, (b) **2-Y**, and (c) **3-Y**. Bolded bonds highlight metal-oxo bonds. Mn (green), O (red), N (blue), Y (purple).

DOI: 10.1021/acs.inorgchem.9b00510
Inorg. Chem. 2019, 58, 14998−15003

Y can be attributed to the increased effective basicity of the ligand framework.

Comparing the structures of **1-Y** and **3-Y**, a more significant contraction in the average Y-oxo and Y−Mn distances is observed in **3-Y** by about 0.1 and 0.15 Å, respectively. This contraction in **3-Y** can be attributed to the geometric pressure exerted by the chelating tripodal tris-amidate ligand framework, pulling the Y center closer to the Mn_3 core than the thermodynamic distances observed in **1-Y** and **2-Y**. Despite the increase in ligand basicity going from acetates to amidates, the shorter Y-oxo interactions enforced by the chelating ligand framework increase the reduction potential of **3-Y**, potentially by decreasing the electron density available for the Mn centers as a consequence of the shorter, stronger Y-oxo interactions. The Y center in **3-Y** is effectively more Lewis acidic because of its closer proximity to the redox sites (Mn_3O_4) enforced by the ligand. In the series of $[Mn_4O_4]$ complexes **1-Mn** ∼ **4-Mn**, noticeable changes in the $[Mn_4O_4]$ core enforced by the chelating ligand have not been observed (Table S2).[56] By taking into account only the basicity of the triamidate ligand ($Ntriam^{3-}$), the reduction potential of **3-Y** would be expected to be close to −1000 mV vs Fc/Fc^+, implying that small geometrical changes (0.1/0.15 Å) in the Y-oxo/Y−Mn distances may shift the cluster redox potential by ∼700 mV. Finally, compared with **1-Y-red** and **1-Y** which display nonchelating ligands on Y, the structure of **3-Y** has Y-oxo/Y−Mn distances more similar to the reduced cluster, **1-Y-red**, suggesting that the $[Ntriam]^{3-}$ ligand enforces a geometry closer to the preferred thermodynamic structure of the reduced $[YMn_3O_4]$ core. Therefore, the geometric pressure imposed by the ligand favors the reduced form, as highlighted by the more positive potential, despite the significantly more electron-rich ligand set.

In summary, $[Mn_4O_4]$ and $[YMn_3O_4]$ complexes featuring bridging ligands of different basicity and chelating properties were synthesized and characterized by X-ray crystallography and cyclic voltammetry. In agreement with previous studies of $[Co_4O_4]$ clusters, increasing the effective basicity of the ligand framework of $[Mn_4O_4]$ results in a decrease of cluster reduction potential.[57] Ligand-induced distortion of cluster geometry is demonstrated as a mode of tuning cluster reduction potential. A significant contraction of Y-oxo/Y−Mn distances by 0.1/0.15 Å enforced by the chelating ligand results in a positive shift of the cluster reduction potential even in the presence of electron donating tris-amidate donors. We propose that within the rigid cavity surrounding the OEC,[23,65] structural changes that affect Ca-oxo/Ca−Mn distances may have a similar effect in tuning the redox potential of the OEC. Furthermore, our model studies suggest that the cation size dependence in the $S_1 \rightarrow S_2$ one e^- oxidation in the OEC is the result of redox tuning through a similar geometric effect: the rigid cavity surrounding the OEC may enforce shorter, nonequilibrium metal-oxo distances for cations with ionic radii larger than that of Ca^{2+}, resulting in an increase in the reduction potential of the OEC and inhibiting the $S_1 \rightarrow S_2$ transition. While other factors such as the pK_a of the water bound to the redox-inactive metal may contribute to the slower turnover frequency of the Sr-substituted OEC, a similar size effect on redox chemistry may also be in place.[66,67] Related geometric constraints in synthetic systems may result in nonlinear changes of reduction potentials and reactivity.

■ ASSOCIATED CONTENT

Supporting Information

The Supporting Information is available free of charge on the ACS Publications website at DOI: 10.1021/acs.inorgchem.9b00510.

Experimental procedures, characterization, and crystal refinement data (PDF)

Accession Codes

CCDC 1897117−1897119 contain the supplementary crystallographic data for this paper. These data can be obtained free of charge via www.ccdc.cam.ac.uk/data_request/cif, by emailing data_request@ccdc.cam.ac.uk, or by contacting The Cambridge Crystallographic Data Centre, 12 Union Road, Cambridge CB2 1EZ, UK; fax: +44 1223 336033.

■ AUTHOR INFORMATION

Corresponding Author

*E-mail: agapie@caltech.edu.

ORCID

Theodor Agapie: 0000-0002-9692-7614

Notes

The authors declare no competing financial interest.

■ ACKNOWLEDGMENTS

This research was supported by the NIH (R01-GM102687B), the Dreyfus Teacher-Scholar Program (T.A.), and Dow Next Generation Educator (instrumentation).

■ REFERENCES

(1) Gray, H. B.; Winkler, J. R. Electron Transfer in Proteins. *Annu. Rev. Biochem.* **1996**, *65*, 537.

(2) Solomon, E. I.; Heppner, D. E.; Johnston, E. M.; Ginsbach, J. W.; Cirera, J.; Qayyum, M.; Kieber-Emmons, M. T.; Kjaergaard, C. H.; Hadt, R. G.; Tian, L. Copper Active Sites in Biology. *Chem. Rev.* **2014**, *114*, 3659.

(3) Liu, J.; Chakraborty, S.; Hosseinzadeh, P.; Yu, Y.; Tian, S.; Petrik, I.; Bhagi, A.; Lu, Y. Metalloproteins Containing Cytochrome, Iron−Sulfur, or Copper Redox Centers. *Chem. Rev.* **2014**, *114*, 4366.

(4) Dennison, C. Investigating the structure and function of cupredoxins. *Coord. Chem. Rev.* **2005**, *249*, 3025.

(5) Dawson, J. H. Probing structure-function relations in heme-containing oxygenases and peroxidases. *Science* **1988**, *240*, 433.

(6) Cowan, J. A.; Lui, S. M., Structure-Function Correlations in High-Potential Iron Proteins. In *Adv. Inorg. Chem.*; Sykes, A. G., Ed.; Academic Press: 1998; Vol. *45*, p 313.

(7) Backes, G.; Mino, Y.; Loehr, T. M.; Meyer, T. E.; Cusanovich, M. A.; Sweeney, W. V.; Adman, E. T.; Sanders-Loehr, J. The environment of Fe_4S_4 clusters in ferredoxins and high-potential iron proteins. New information from x-ray crystallography and resonance Raman spectroscopy. *J. Am. Chem. Soc.* **1991**, *113*, 2055.

(8) Garner, D. K.; Vaughan, M. D.; Hwang, H. J.; Savelieff, M. G.; Berry, S. M.; Honek, J. F.; Lu, Y. Reduction Potential Tuning of the Blue Copper Center in Pseudomonas aeruginosa Azurin by the Axial Methionine as Probed by Unnatural Amino Acids. *J. Am. Chem. Soc.* **2006**, *128*, 15608.

(9) Werth, M. T.; Cecchini, G.; Manodori, A.; Ackrell, B. A.; Schröder, I.; Gunsalus, R. P.; Johnson, M. K. Site-directed mutagenesis of conserved cysteine residues in Escherichia coli fumarate reductase: modification of the spectroscopic and electrochemical properties of the [2Fe-2S] cluster. *Proc. Natl. Acad. Sci. U. S. A.* **1990**, *87*, 8965.

(10) Birrell, J. A.; Laurich, C.; Reijerse, E. J.; Ogata, H.; Lubitz, W. Importance of Hydrogen Bonding in Fine Tuning the [2Fe-2S]

DOI: 10.1021/acs.inorgchem.9b00510
Inorg. Chem. 2019, 58, 14998−15003

Cluster Redox Potential of HydC from Thermotoga maritima. *Biochemistry* **2016**, *55*, 4344.
(11) Hadt, R. G.; Sun, N.; Marshall, N. M.; Hodgson, K. O.; Hedman, B.; Lu, Y.; Solomon, E. I. Spectroscopic and DFT Studies of Second-Sphere Variants of the Type 1 Copper Site in Azurin: Covalent and Nonlocal Electrostatic Contributions to Reduction Potentials. *J. Am. Chem. Soc.* **2012**, *134*, 16701.
(12) Dey, A.; Jenney, F. E.; Adams, M. W. W.; Babini, E.; Takahashi, Y.; Fukuyama, K.; Hodgson, K. O.; Hedman, B.; Solomon, E. I. Solvent Tuning of Electrochemical Potentials in the Active Sites of HiPIP Versus Ferredoxin. *Science* **2007**, *318*, 1464.
(13) Low, D. W.; Hill, M. G. Backbone-Engineered High-Potential Iron Proteins: Effects of Active-Site Hydrogen Bonding on Reduction Potential. *J. Am. Chem. Soc.* **2000**, *122*, 11039.
(14) Tezcan, F. A.; Winkler, J. R.; Gray, H. B. Effects of Ligation and Folding on Reduction Potentials of Heme Proteins. *J. Am. Chem. Soc.* **1998**, *120*, 13383.
(15) Brinkert, K.; De Causmaecker, S.; Krieger-Liszkay, A.; Fantuzzi, A.; Rutherford, A. W. Bicarbonate-induced redox tuning in Photosystem II for regulation and protection. *Proc. Natl. Acad. Sci. U. S. A.* **2016**, *113*, 12144.
(16) Pantazis, D. A. Missing Pieces in the Puzzle of Biological Water Oxidation. *ACS Catal.* **2018**, *8*, 9477.
(17) Shen, J.-R. The Structure of Photosystem II and the Mechanism of Water Oxidation in Photosynthesis. *Annu. Rev. Plant Biol.* **2015**, *66*, 23.
(18) Yano, J.; Yachandra, V. Mn_4Ca Cluster in Photosynthesis: Where and How Water is Oxidized to Dioxygen. *Chem. Rev.* **2014**, *114*, 4175.
(19) Cox, N.; Pantazis, D. A.; Neese, F.; Lubitz, W. Biological Water Oxidation. *Acc. Chem. Res.* **2013**, *46*, 1588.
(20) Cox, N.; Retegan, M.; Neese, F.; Pantazis, D. A.; Boussac, A.; Lubitz, W. Electronic structure of the oxygen-evolving complex in photosystem II prior to O-O bond formation. *Science* **2014**, *345*, 804.
(21) Kulik, L. V.; Epel, B.; Lubitz, W.; Messinger, J. Electronic Structure of the Mn_4O_xCa Cluster in the S_0 and S_2 States of the Oxygen-Evolving Complex of Photosystem II Based on Pulse ^{55}Mn-ENDOR and EPR Spectroscopy. *J. Am. Chem. Soc.* **2007**, *129*, 13421.
(22) Lee, C.-I.; Lakshmi, K. V.; Brudvig, G. W. Probing the Functional Role of Ca^{2+} in the Oxygen-Evolving Complex of Photosystem II by Metal Ion Inhibition. *Biochemistry* **2007**, *46*, 3211.
(23) Lohmiller, T.; Shelby, M. L.; Long, X.; Yachandra, V. K.; Yano, J. Removal of Ca^{2+} from the Oxygen-Evolving Complex in Photosystem II Has Minimal Effect on the Mn_4O_5 Core Structure: A Polarized Mn X-ray Absorption Spectroscopy Study. *J. Phys. Chem. B* **2015**, *119*, 13742.
(24) Miqyass, M.; Marosvölgyi, M. A.; Nagel, Z.; Yocum, C. F.; van Gorkom, H. J. S-State Dependence of the Calcium Requirement and Binding Characteristics in the Oxygen-Evolving Complex of Photosystem II. *Biochemistry* **2008**, *47*, 7915.
(25) Pantazis, D. A.; Ames, W.; Cox, N.; Lubitz, W.; Neese, F. Two Interconvertible Structures that Explain the Spectroscopic Properties of the Oxygen-Evolving Complex of Photosystem II in the S_2 State. *Angew. Chem., Int. Ed.* **2012**, *51*, 9935.
(26) Peloquin, J. M.; Campbell, K. A.; Randall, D. W.; Evanchik, M. A.; Pecoraro, V. L.; Armstrong, W. H.; Britt, R. D. ^{55}Mn ENDOR of the S_2-State Multiline EPR Signal of Photosystem II: Implications on the Structure of the Tetranuclear Mn Cluster. *J. Am. Chem. Soc.* **2000**, *122*, 10926.
(27) Vrettos, J. S.; Stone, D. A.; Brudvig, G. W. Quantifying the Ion Selectivity of the Ca^{2+} Site in Photosystem II: Evidence for Direct Involvement of Ca^{2+} in O_2 Formation. *Biochemistry* **2001**, *40*, 7937.
(28) Siegbahn, P. E. M. Structures and Energetics for O_2 Formation in Photosystem II. *Acc. Chem. Res.* **2009**, *42*, 1871.
(29) Siegbahn, P. E. M.; Crabtree, R. H. Manganese Oxyl Radical Intermediates and O−O Bond Formation in Photosynthetic Oxygen Evolution and a Proposed Role for the Calcium Cofactor in Photosystem II. *J. Am. Chem. Soc.* **1999**, *121*, 117.
(30) Mukherjee, S.; Stull, J. A.; Yano, J.; Stamatatos, T. C.; Pringouri, K.; Stich, T. A.; Abboud, K. A.; Britt, R. D.; Yachandra, V. K.; Christou, G. Synthetic model of the asymmetric $[Mn_3CaO_4]$ cubane core of the oxygen-evolving complex of photosystem II. *Proc. Natl. Acad. Sci. U. S. A.* **2012**, *109*, 2257.
(31) Tsui, E. Y.; Tran, R.; Yano, J.; Agapie, T. Redox-inactive metals modulate the reduction potential in heterometallic manganese−oxido clusters. *Nat. Chem.* **2013**, *5*, 293.
(32) Zhang, C.; Chen, C.; Dong, H.; Shen, J.-R.; Dau, H.; Zhao, J. A synthetic Mn_4Ca-cluster mimicking the oxygen-evolving center of photosynthesis. *Science* **2015**, *348*, 690.
(33) Vaddypally, S.; Kondaveeti, S. K.; Karki, S.; Van Vliet, M. M.; Levis, R. J.; Zdilla, M. J. Reactive Pendant Mn = O in a Synthetic Structural Model of a Proposed S4 State in the Photosynthetic Oxygen Evolving Complex. *J. Am. Chem. Soc.* **2017**, *139*, 4675.
(34) Ono, T.-a.; Rompel, A.; Mino, H.; Chiba, N. Ca2+ Function in Photosynthetic Oxygen Evolution Studied by Alkali Metal Cations Substitution. *Biophys. J.* **2001**, *81*, 1831.
(35) Boussac, A.; Rutherford, A. W. Nature of the inhibition of the oxygen-evolving enzyme of photosystem II induced by sodium chloride washing and reversed by the addition of Ca^{2+} or Sr^{2+}. *Biochemistry* **1988**, *27*, 3476.
(36) Herbert, D. E.; Lionetti, D.; Rittle, J.; Agapie, T. Heterometallic Triiron-Oxo/Hydroxo Clusters: Effect of Redox-Inactive Metals. *J. Am. Chem. Soc.* **2013**, *135*, 19075.
(37) Kanady, J. S.; Tsui, E. Y.; Day, M. W.; Agapie, T. A Synthetic Model of the Mn_3Ca Subsite of the Oxygen-Evolving Complex in Photosystem II. *Science* **2011**, *333*, 733.
(38) Lin, P.-H.; Takase, M. K.; Agapie, T. Investigations of the Effect of the Non-Manganese Metal in Heterometallic-Oxido Cluster Models of the Oxygen Evolving Complex of Photosystem II: Lanthanides as Substitutes for Calcium. *Inorg. Chem.* **2015**, *54*, 59.
(39) Tsui, E. Y.; Agapie, T. Reduction potentials of heterometallic manganese−oxido cubane complexes modulated by redox-inactive metals. *Proc. Natl. Acad. Sci. U. S. A.* **2013**, *110*, 10084.
(40) Lionetti, D.; Suseno, S.; Tsui, E. Y.; Lu, L.; Stich, T. A.; Carsch, K. M.; Nielsen, R. J.; Goddard, W. A.; Britt, R. D.; Agapie, T. Effects of Lewis Acidic Metal Ions (M) on Oxygen-Atom Transfer Reactivity of Heterometallic Mn3MO4 Cubane and Fe3MO(OH) and Mn3MO(OH) Clusters. *Inorg. Chem.* **2019**, *58*, 2336.
(41) Gerey, B.; Gouré, E.; Fortage, J.; Pécaut, J.; Collomb, M.-N. Manganese-calcium/strontium heterometallic compounds and their relevance for the oxygen-evolving center of photosystem II. *Coord. Chem. Rev.* **2016**, *319*, 1.
(42) Krewald, V.; Neese, F.; Pantazis, D. A. Redox potential tuning by redox-inactive cations in nature's water oxidizing catalyst and synthetic analogues. *Phys. Chem. Chem. Phys.* **2016**, *18*, 10739.
(43) Bang, S.; Lee, Y.-M.; Hong, S.; Cho, K.-B.; Nishida, Y.; Seo, M. S.; Sarangi, R.; Fukuzumi, S.; Nam, W. Redox-inactive metal ions modulate the reactivity and oxygen release of mononuclear non-haem iron(III)−peroxo complexes. *Nat. Chem.* **2014**, *6*, 934.
(44) Chantarojsiri, T.; Ziller, J. W.; Yang, J. Y. Incorporation of redox-inactive cations promotes iron catalyzed aerobic C−H oxidation at mild potentials. *Chem. Sci.* **2018**, *9*, 2567.
(45) Park, Y. J.; Ziller, J. W.; Borovik, A. S. The Effects of Redox-Inactive Metal Ions on the Activation of Dioxygen: Isolation and Characterization of a Heterobimetallic Complex Containing a Mn^{III}−(μ-OH)−Ca^{II} Core. *J. Am. Chem. Soc.* **2011**, *133*, 9258.
(46) Reath, A. H.; Ziller, J. W.; Tsay, C.; Ryan, A. J.; Yang, J. Y. Redox Potential and Electronic Structure Effects of Proximal Nonredox Active Cations in Cobalt Schiff Base Complexes. *Inorg. Chem.* **2017**, *56*, 3713.
(47) Leeladee, P.; Baglia, R. A.; Prokop, K. A.; Latifi, R.; de Visser, S. P.; Goldberg, D. P. Valence Tautomerism in a High-Valent Manganese−Oxo Porphyrinoid Complex Induced by a Lewis Acid. *J. Am. Chem. Soc.* **2012**, *134*, 10397.
(48) Miller, C. G.; Gordon-Wylie, S. W.; Horwitz, C. P.; Strazisar, S. A.; Peraino, D. K.; Clark, G. R.; Weintraub, S. T.; Collins, T. J. A

DOI: 10.1021/acs.inorgchem.9b00510
Inorg. Chem. 2019, 58, 14998−15003

Method for Driving O-Atom Transfer: Secondary Ion Binding to a Tetraamide Macrocyclic Ligand. *J. Am. Chem. Soc.* **1998**, *120*, 11540.
(49) Park, Y. J.; Cook, S. A.; Sickerman, N. S.; Sano, Y.; Ziller, J. W.; Borovik, A. S. Heterobimetallic complexes with MIII-(μ-OH)-MII cores (MIII = Fe, Mn, Ga; MII = Ca, Sr, and Ba): structural, kinetic, and redox properties. *Chem. Sci.* **2013**, *4*, 717.
(50) Du, H.; Lo, P.-K.; Hu, Z.; Liang, H.; Lau, K.-C.; Wang, Y.-N.; Lam, W. W. Y.; Lau, T.-C. Lewis acid-activated oxidation of alcohols by permanganate. *Chem. Commun.* **2011**, *47*, 7143.
(51) Kanady, J. S.; Mendoza-Cortes, J. L.; Tsui, E. Y.; Nielsen, R. J.; Goddard, W. A.; Agapie, T. Oxygen Atom Transfer and Oxidative Water Incorporation in Cuboidal Mn_3MO_n Complexes Based on Synthetic, Isotopic Labeling, and Computational Studies. *J. Am. Chem. Soc.* **2013**, *135*, 1073.
(52) Fukuzumi, S.; Ohkubo, K.; Lee, Y.-M.; Nam, W. Lewis Acid Coupled Electron Transfer of Metal−Oxygen Intermediates. *Chem. - Eur. J.* **2015**, *21*, 17548.
(53) Bae, S. H.; Lee, Y.-M.; Fukuzumi, S.; Nam, W. Fine Control of the Redox Reactivity of a Nonheme Iron(III)−Peroxo Complex by Binding Redox-Inactive Metal Ions. *Angew. Chem., Int. Ed.* **2017**, *56*, 801.
(54) VanGelder, L. E.; Brennessel, W. W.; Matson, E. M. Tuning the redox profiles of polyoxovanadate-alkoxide clusters via heterometal installation: toward designer redox Reagents. *Dalton Trans* **2018**, *47*, 3698.
(55) Meyer, R. L.; Brennessel, W. W.; Matson, E. M. Synthesis of a gallium-functionalized polyoxovanadate-alkoxide cluster: Toward a general route for heterometal installation. *Polyhedron* **2018**, *156*, 303.
(56) Lee, H. B.; Shiau, A. A.; Oyala, P. H.; Marchiori, D. A.; Gul, S.; Chatterjee, R.; Yano, J.; Britt, R. D.; Agapie, T. Tetranuclear $[Mn^{III}Mn_3^{IV}O_4]$ Complexes as Spectroscopic Models of the S_2 State of the Oxygen Evolving Complex in Photosystem II. *J. Am. Chem. Soc.* **2018**, *140*, 17175.
(57) Nguyen, A. I.; Wang, J.; Levine, D. S.; Ziegler, M. S.; Tilley, T. D. Synthetic control and empirical prediction of redox potentials for Co_4O_4 cubanes over a 1.4 V range: implications for catalyst design and evaluation of high-valent intermediates in water oxidation. *Chem. Sci.* **2017**, *8*, 4274.
(58) Bordwell, F. G.; Algrim, D. Nitrogen acids. 1. Carboxamides and sulfonamides. *J. Org. Chem.* **1976**, *41*, 2507.
(59) Hansch, C.; Leo, A.; Taft, R. W. A survey of Hammett substituent constants and resonance and field parameters. *Chem. Rev.* **1991**, *91*, 165.
(60) Kütt, A.; Leito, I.; Kaljurand, I.; Sooväli, L.; Vlasov, V. M.; Yagupolskii, L. M.; Koppel, I. A. A Comprehensive Self-Consistent Spectrophotometric Acidity Scale of Neutral Brønsted Acids in Acetonitrile. *J. Org. Chem.* **2006**, *71*, 2829.
(61) Bordwell, F. G.; Harrelson, J. A.; Lynch, T. Y. Homolytic bond dissociation energies for the cleavage of α-N-H bonds in carboxamides, sulfonamides, and their derivatives. The question of synergism in nitrogen-centered radicals. *J. Org. Chem.* **1990**, *55*, 3337.
(62) Lin, P.-H.; Tsui, E. Y.; Habib, F.; Murugesu, M.; Agapie, T. Effect of the Mn Oxidation State on Single-Molecule-Magnet Properties: Mn^{III} vs Mn^{IV} in Biologically Inspired $DyMn_3O_4$ Cubanes. *Inorg. Chem.* **2016**, *55*, 6095.
(63) Kanady, J. S.; Lin, P.-H.; Carsch, K. M.; Nielsen, R. J.; Takase, M. K.; Goddard, W. A.; Agapie, T. Toward Models for the Full Oxygen-Evolving Complex of Photosystem II by Ligand Coordination To Lower the Symmetry of the Mn_3CaO_4 Cubane: Demonstration That Electronic Effects Facilitate Binding of a Fifth Metal. *J. Am. Chem. Soc.* **2014**, *136*, 14373.
(64) Bordwell, F. G.; Ji, G. Z. Equilibrium acidities and homolytic bond dissociation energies of the H-O bonds in oximes and amidoximes. *J. Org. Chem.* **1992**, *57*, 3019.
(65) Davis, K. M.; Pushkar, Y. N. Structure of the Oxygen Evolving Complex of Photosystem II at Room Temperature. *J. Phys. Chem. B* **2015**, *119*, 3492.
(66) Koua, F. H. M.; Umena, Y.; Kawakami, K.; Shen, J.-R. Structure of Sr-substituted photosystem II at 2.1 Å resolution and its implications in the mechanism of water oxidation. *Proc. Natl. Acad. Sci. U. S. A.* **2013**, *110*, 3889.
(67) Boussac, A.; Ugur, I.; Marion, A.; Sugiura, M.; Kaila, V. R. I.; Rutherford, A. W. The low spin - high spin equilibrium in the S2-state of the water oxidizing enzyme. *Biochim. Biophys. Acta, Bioenerg.* **2018**, *1859*, 342.

DOI: 10.1021/acs.inorgchem.9b00510
Inorg. Chem. 2019, 58, 14998−15003